Journal of Applied Mechanics and Technical Physics, Vol. 46, No. 1, pp. 21–32, 2005

GAS DYNAMICS OF A LOW-PRESSURE CHAMBER IN A HIGH-ENTHALPY SHORT-DURATION WIND TUNNEL

V. V. Shumskii and M. I. Yaroslavtsev

UDC 629.7.036.2; 533.607

Gas dynamics of a low-pressure chamber in a double-chamber hotshot wind tunnel is considered. The time needed to fill the second chamber is in good agreement with the value obtained by examining the quasi-steady process of emptying and filling of the high-pressure and low-pressure chambers. The transitional process is strongly affected by wave processes in the channel between the chambers. By changing the place of the throttling grid in this channel, one can change the time of filling of the second chamber (decrease it severalfold). The examined schemes of air input into the second chamber ensure its complete deceleration. The Mach number at the exit of the second chamber (in the wind-tunnel nozzle throat) is almost constant over the cross section and close to unity.

Key words: *high-enthalpy wind tunnel, double chamber, test gas.*

Introduction. In investigations with high-velocity air flows and gas-dynamic models with combustion, one has not only to ensure similarity criteria typical of an aerodynamic experiment but also reproduce full-scale values of pressure p, temperature T, and enthalpy [1–4]. The reason is that the conditions of ignition, especially self-ignition, and the laws of heat release along the combustion chamber, which determine the force characteristics of the model, significantly depend on pressure and temperature.

To reproduce full-scale flight parameters with a Mach number M = 4–5 and dynamic pressure $q = 0.6$–1 bar in high-enthalpy short-duration facilities with a plenum chamber volume of 10 dm^3 and nozzle-exit diameter of 300–400 mm, one needs a double plenum chamber to retain the test time at a level of 0.1–0.2 sec. This time is acceptable from the viewpoint of stabilization of the basic gas-thermodynamic processes in models and high-quality measurements of pressures, forces, flow rates, and heat fluxes.

A layout of a double (two-section) plenum chamber for expanding the capabilities of short-time facilities was proposed in [5, 6]. The use of such a chamber, however, is most efficient in facilities with a "plateau" of physical parameters during the test time under the condition that the first chamber can ensure a pressure much higher than the pressure necessary to simulate the stagnation pressure in the flow incoming onto the model tested. An example of such a facility is the IT-302M hypersonic wind tunnel based at the Institute of Theoretical and Applied Mechanics of the Siberian Branch of the Russian Academy of Sciences [4, 7, 8].

The layout of the facility is shown in Fig. 1. In the high-pressure chamber, the test-gas parameters are changed isochorically (due to heat addition) from $p_{\mathrm{ch1,(pump)}}$ and $T_{\mathrm{ch1,(pump)}}$ to $p_{\mathrm{ch1,(0)}}$ and $T_{\mathrm{ch1,(0)}}$ after heat addition. Hereinafter, the subscript (pump) refers to parameters of pumping of the test gas into the first chamber before the experiment and the subscript (0) refers to parameters at the time $\tau = 0$ (the beginning of the test time $\tau = 0$ is assumed to be the moment of diaphragm breakdown); if the test-gas parameters are used without any subscripts, this means that the parameters refer to all instants during the test time τ.

After breakdown of diaphragm 4 (see Fig. 1), the test gas enters the low-pressure chamber located directly upstream of the nozzle. As the pressure p_{ch1} in the first chamber is much higher than the pressure p_{ch2} in the second chamber ($p_{\mathrm{ch1}} \gg p_{\mathrm{ch2}} = p_{0,\mathrm{flight}}$), the area of orifices between the chambers F_{1-2} is smaller than the nozzle-throat

Institute of Theoretical and Applied Mechanics, Siberian Division, Russian Academy of Sciences, Novosibirsk 630090; shymsky@itam.nsc.ru; yaroslav@itam.nsc.ru. Translated from Prikladnaya Mekhanika i Tekhnicheskaya Fizika, Vol. 46, No. 1, pp. 29–43, January–February, 2005. Original article submitted January 15, 2004; revision submitted May 25, 2004.

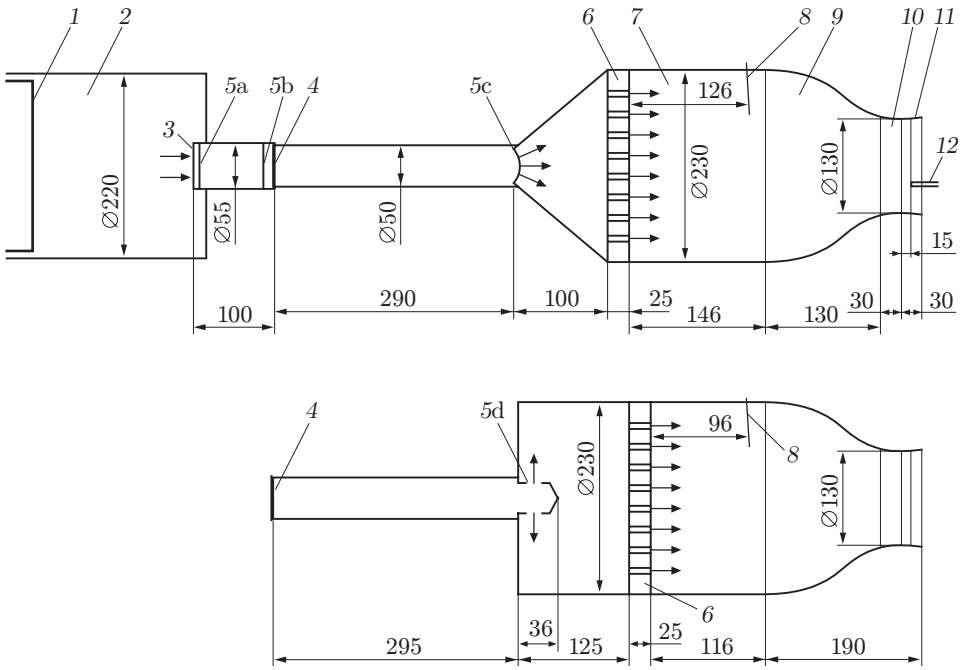

Fig. 1. Layout of the wind tunnel: 1) plunger of the pressure multiplier; 2) first chamber; 3) impingement plate; 4) diaphragm; 5) throttling grid between the chambers (the letters a–d indicate the positions of the throttling grid between the chambers in different tests); 6) throttling grid in the second chamber; 7) second chamber; 8) cross section in the second chamber where the static and total pressures were measured; 9) subsonic Vitoshinskii nozzle; 10) throat section; 11) expanding section with a 5° angle of the generatrix to the centerline; 12) total pressure probe.

cross-sectional area F_{th} approximately by a factor of $p_{\text{ch1}}/p_{\text{ch2}}$. This fact is responsible for the increase in the test time approximately by a factor of F_{th}/F_{1-2} as compared to the single plenum chamber in which $p_{\text{ch1}} = p_{0,\text{flight}}$. Here, $p_{0,\text{flight}}$ is the full-scale stagnation pressure in flight of a full-scale object.

The gas dynamics of the second chamber was examined with allowance for specific features of the IT-302M wind tunnel.

For the test time to be longer, the pressure in the first chamber should be as close as possible to the maximum admissible value. The maximum admissible value in IT-302M is $p_{\text{ch1}} = 1000$ bars. Simultaneously, the full-scale pressure for M $= 4$ and $q = 0.6$–1 bar is 8–13 bars, i.e., the degree of throttling should be close to 100.

The following elements are located between the chambers: impingement plate 3 quenching the action of the shock-wave in the case of pulse addition of heat in the first chamber, diaphragm 4, and throttling grid 5 with the cross-sectional area F_{1-2} of orifices where the test gas is throttled from the pressure p_{ch1} to the pressure p_{ch2}. Thus, it is difficult to avoid a channel between the chambers, where diaphragm breakdown can initiate wave processes.

The second-chamber diameter should be greater than the nozzle-throat diameter at least by a factor of 2 to 3 [9]. In reproducing full-scale flight parameters with M $= 4$, this makes the volumes of the first and second chambers commensurable for nozzles with exit diameters of 300–400 mm, and the length of the second chamber is almost equal to its diameter.

All this creates problems with test-gas inflow into the second chamber, filling of the chamber, and uniformity of the flowfield at the chamber exit (at the entrance of the wind-tunnel nozzle).

To study the issues mentioned above, we considered gas dynamics of processes in the second chamber of the IT-302M wind tunnel, beginning from diaphragm breakdown to the end of the test time.

The use of high-enthalpy short-duration facilities for investigating gas-dynamic models with combustion in the hypersonic range of velocities ensures full-scale values of stagnation pressure and enthalpy (temperature) and Mach and Reynolds numbers simultaneously, which is next to impossible in blowdown facilities. For this reason, many studies are performed to expand the capabilities of such facilities and to improve the accuracy and information value of measurements in such wind tunnels (see, e.g., reviews [10, 11]).

Layout of the Experiment. The layout of the experiments is clear from Fig. 1, which shows the relative positions of various elements of the plenum chamber in the experiments conducted. In the variant of the second chamber in the upper figure, the test gas is injected into the second chamber in a distributed manner from the direction parallel to the centerline to the direction of the generatrix of the frontal cover; this is valid for all positions of the throttling grid (5a, 5b, and 5c). The lower figure shows the second-chamber variant with a stagnant zone in the front part of the chamber. In this variant, the test gas is injected into the stagnant zone perpendicular to the chamber axis through orifices in the throttling grid 5d. All the elements in the lower figure are the same as those in the upper figure, except for the throttling grids 5a, 5b, and 5c (no tests with the lower variant of the chamber were performed with these positions of the grids).

The test gas was air. Heat addition in the first chamber in the process with $V = \text{const}$ was performed owing to a capacitor discharge. The charging voltage was $U = 4$ kV, which corresponded to an energy contribution of approximately 0.6 MJ.

The experiments were performed with the first chamber volume $V_{\text{ch1}} = 9.6$ dm^3 and the pressure of air pumping $p_{\text{ch1,(pump)}} = 80$ bars. The volume of the second chamber was $V_{\text{ch2}} \approx 12$ dm^3 (it could be slightly changed by using different frontal covers — see the upper and lower drawings in Fig. 1).

The throttling grid had seven orifices 3.8 mm in diameter with a total area $F_{1-2} = 0.79$ cm^2 ($F_{\text{th}}/F_{1-2} = 167$). The throttling grid was mounted in different cross sections to find the influence of its position on the transitional process during filling of the second chamber.

An additional throttling grid (143 orifices 5 mm in diameter; see 6 in Fig. 1) was mounted in the second chamber in the first experiments. It was assumed that this grid would be responsible for partial throttling of pressure between the chambers to have smaller distortions of the flow in the second chamber owing to inflow of a strongly underexpanded jet. It turned out, however, that there was no need in this additional grid. Therefore, in subsequent experiments, the orifices in grid 6 were drilled out to a diameter of 14.5 mm (the total area of orifices normalized to the cross-sectional area of the second chamber was $f = 0.55$). The new role of this grid was flow equalization [12, 13] with a moderate pressure difference on the grid (about 0.15 bar) and a hydraulic resistance coefficient $\zeta \approx 2.2$ [13]. Thus, recommendations of Taganov [12] on the optimal value of ζ for the equalizing grid were satisfied. Some experiments were performed without this grid.

The cylindrical part of the second chamber ended by the Vitoshinskii nozzle [14] with a nozzle-throat diameter of 130 mm. The length of the throat section was chosen with allowance for recommendations of [14] and reached approximately 25% of the nozzle-throat diameter. The nozzle exit had a short expanding conical section 11 with a 5° angle of inclination of the generatrix to the axis to prevent distortion of the velocity profile in the throat section because of boundary-layer "bleeding" [15].

The readings of pressure probes were registered in experiments. As the velocities in the first chamber are low, the pressure measured on the wall was assumed to be the total pressure p_{ch1}. The parameters measured in the second chamber in cross section 8 (Fig. 1) were the static pressure and the stagnation pressure p_{ch2} (by a total pressure probe). The static pressure in the nozzle-throat cross section was also measured. The field of stagnation pressures was measured by a cross-shaped rake of total pressure probes at seven points at the exit of the second chamber. The measurement system contained a digital device, which registered the readings of pressure probes every 0.2–0.4 msec.

The use of a pressure multiplier [4, 7, 10, 16] ensured constant physical parameters of the flow incoming onto the model or their variation by a prescribed law. The present experiments were performed with and without the pressure multiplier. In experiments without the pressure multiplier, plunger 1 (Fig. 1) was located in the extreme rear position in the first chamber. In these experiments, the wind tunnel operated in the classical hotshot mode [6] with flow exhaustion from a constant-volume tank and physical parameters of the test gas decreasing during the test time. In experiments with the pressure multiplier, the pressure ahead of the large piston of the multiplier was chosen such that it ensured the condition $p_{\text{ch1}}(\tau) = \text{const}$ or an increase in the dependence $p_{\text{ch1}}(\tau)$ during the test time. For these three cases, Fig. 2 shows typical dependences $p_{\text{ch1}}(\tau)$. Curve 1 corresponds to wind-tunnel operation without the pressure multiplier. Therefore, the pressure in this experiment decreases during the test time. In the experiment described by curve 2, the pressure was maintained constant during the test time due to operation of the pressure multiplier. In the experiment described by curve 3, the pressure ahead of the large piston of the pressure multiplier was higher than that required to sustain a constant pressure. Therefore, the plunger of the pressure

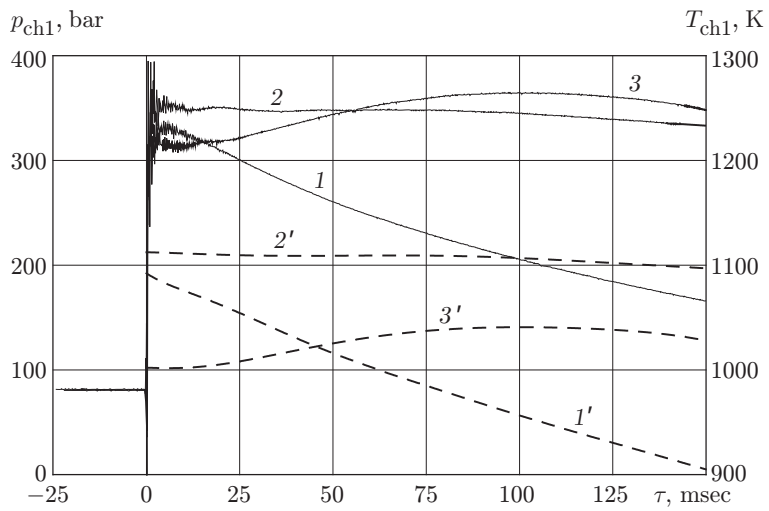

Fig. 2. Pressure in the first chamber registered by the measurement system during the test time (curves 1–3) and the corresponding values of temperature T_{ch1} (curves $1'$–$3'$).

multiplier adiabatically compressed air in the first chamber, and the pressure in the first chamber increased during a certain time.

Figure 2 shows the temperature versus the test time for the same experiments. The character of the dependence $T_{\text{ch1}}(\tau)$ corresponds to the changes in $p_{\text{ch1}}(\tau)$. For instance, in the experiment described by curve $3'$, the temperature increases in the part of the test time when an increase in pressure is observed. Note, the regime with a higher pressure ahead of the piston of the pressure multiplier than that required to maintain constant parameters in the first chamber can be used if it is necessary to heat the test gas to a temperature higher than the level corresponding to the capacitor energy. If the facility is equipped by a device for deliberate breakdown of the diaphragm, the test gas in the first chamber is additionally compressed after heat addition even before diaphragm breakdown, owing to the high pressure ahead of the pressure-multiplier piston. Such an operation regime of the wind tunnel can also be achieved in principle without external heat addition from the capacitor discharge (in a regime of purely adiabatic compression). In this case, either the test time decreases or smaller nozzles should be used.

Thus, we considered the entire range of variation of test-gas parameters: with parameters decreasing during the test time, with constant parameters, and with increasing parameters.

The data of the pressure probes were approximated on the interval $[\tau_1, \tau_2]$ by a polynomial of power n. For instance, for the pressure in the first chamber, we have

$$p_{\text{ch1}}(\tau) = a_0 + a_1\tau + a_2\tau^2 + \ldots + a_n\tau^n.$$

The value of n for different experiments and different parameters was varied from 5 to 14. After that, the data of approximation were extended to the interval $[\tau_3, \tau_4]$. For the pressure in the first chamber $\tau_3 = 0$, i.e., it was assumed that $p_{\text{ch1},(0)} = a_0$ (for the remaining parameters, normally, we had $\tau_3 = \tau_1$); $\tau_4 \leqslant \tau_2$.

As an example, Fig. 3 shows the approximation curve for the stagnation pressure in the second chamber. Curve 1 is the pressure recorded directly by the measurement system; curves 2 and 3 are approximation curves. Only the initial interval in the second chamber beginning normally from τ = 3–5 msec and up to τ = 30–60 msec was used to analyze the transitional process (see curve 2 in Fig. 3), because it was important to know the character of filling of the second chamber and the processes in this chamber in the beginning of the test time. To analyze the flow at the exit of the second chamber, the transitional process should be eliminated. Therefore, the interval after the transitional process, beginning from τ = 20–35 msec and to the end of the test time τ = 140–160 msec (see curve 3 in Fig. 3) was used for approximation. The quantity σ characterizes the root-mean-square deviation of the approximation curve from the values measured in the experiment. At the same time, Fig. 2 shows only the values of $p_{\text{ch1}}(\tau)$ recorded by the measurement system (not approximated) because the approximation curves in the scale of this figure coincide with the raw data.

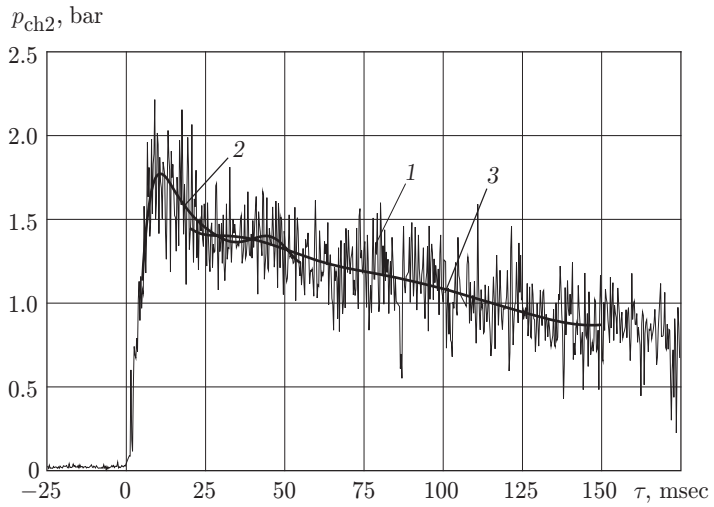

Fig. 3. Stagnation pressure in the second chamber versus the test time τ: 1) pressure registered by the measurement system; 2) approximation: $n = 10$, $[\tau_1, \tau_2] = [5 \text{ msec}, 60 \text{ msec}]$, $[\tau_3, \tau_4] = [5 \text{ msec}, 55 \text{ msec}]$, and $\sigma = 0.212$ bar; 3) approximation: $n = 10$, $[\tau_1, \tau_2] = [20 \text{ msec}, 160 \text{ msec}]$, $[\tau_3, \tau_4] = [20 \text{ msec}, 150 \text{ msec}]$, and $\sigma = 0.174$ bar.

Time of Filling of the Second Chamber. The basic relations associated with filling and emptying of the chambers [17, 18] follow from the equation of conservation of mass during overflow of the test gas from the first chamber to the second one:

$$dG_{ch2} = \dot{G}_{ch1}\, d\tau - \dot{G}_{ch2}\, d\tau. \tag{1}$$

Here G_{ch2} is the mass of the test gas in the second chamber, $\dot{G}_{ch1}$ is the flow rate of the test gas from the first chamber, and $\dot{G}_{ch2}$ is the flow rate from the second chamber.

We use the following assumptions:

— $p_{ch1}(\tau) = \text{const}$ and $T_{ch1}(\tau) = \text{const}$, i.e., the parameters in the first chamber are sustained by the pressure multiplier;

— throttling occurs in the throttling grid located between the chambers;

— $T_{ch2}(\tau) = T_{ch1}(\tau)$ and the ratio of specific heats $k = \text{const}$, i.e., the test gas is assumed to be an ideal gas with the equation of state $pv = RT$ (R is the specific gas constant);

— the flow is quasi-steady, i.e., the parameters of the test gas in the second chamber are constant but change monotonically in time during the chamber-filling process;

— the velocity of the test gas in the orifices of the throttling grid equals the velocity of sound in the entire process of filling of the second chamber;

— sonic exhaustion of the test gas from the second chamber occurs;

— initial pressure in the second chamber (before diaphragm breakdown) equals zero.

Under these assumptions, we obtain

$$\dot{G}_{ch1} = \mu_{1-2} B F_{1-2} p_{ch1} / \sqrt{RT_{ch1}}; \tag{2}$$

$$\dot{G}_{ch2} = \mu_{th} B F_{th} p_{ch2} / \sqrt{RT_{ch2}}, \tag{3}$$

where μ_{1-2} and μ_{th} are the flow-rate coefficients of the throttling orifice and nozzle, respectively;

$$B = \Big(\frac{2}{k+1}\Big)^{1/(k-1)} \sqrt{\frac{2k}{k+1}}.$$

In the quasi-steady regime after completion of all transitional processes of filling of the second chamber (theoretically, at $\tau = \infty$), we have

$$\mu_{1-2} F_{1-2} p_{ch1} = \mu_{th} F_{th} p_{ch2}(\tau = \infty), \tag{4}$$

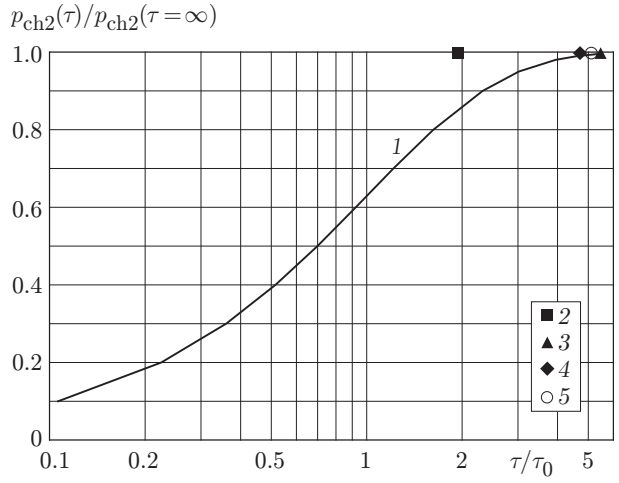

Fig. 4. Pressure in the second chamber (during filling) versus the normalized time $\bar{\tau} = \tau/\tau_0$: curve 1 refers to the calculation by Eq. (6) and points 2–5 refer to the experimental data (averaged over several experiments) obtained with the throttling grid positions 5a–5d (Fig. 1), respectively.

where $p_{ch2}(\tau = \infty)$ is the pressure that will be reached in the second chamber after completion of the transitional processes of chamber filling.

Substituting Eqs. (2) and (3) into Eq. (1) and integrating it from $\tau = 0$ to the current value of τ, we obtain the time of filling of the second chamber up to the pressure $p_{ch2}(\tau)$:

$$\tau = \tau_0 \ln\left(1 - p_{ch2}(\tau)/p_{ch2}(\tau = \infty)\right)^{-1},$$

where τ_0 is the characteristic time of filling of the second chamber equal to

$$\tau_0 = \frac{V_{ch2}}{B\mu_{th}F_{th}\sqrt{RT_{ch1}}} = \frac{V_{ch2}p_{ch2}(\tau = \infty)}{B\mu_{1-2}F_{1-2}p_{ch1}\sqrt{RT_{ch1}}}. \tag{5}$$

The quantity τ_0 is the time necessary to fill the second chamber of volume V_{ch2} to a necessary pressure p_{ch2} if the flow rate of the test gas incoming through orifices with an area F_{1-2} were constant and corresponded to parameters in the first chamber at the time $\tau = 0$ and if there were no exhaustion from the second chamber through the nozzle with an area F_{th}. Thus, the quantity

$$\bar{\tau} = \tau/\tau_0 = \ln\left(1 - p_{ch2}(\tau)/p_{ch2}(\tau = \infty)\right)^{-1} \tag{6}$$

can serve as a similarity criterion. For chambers with different values of F_{th}, V_{ch2}, T_{ch1}, ... , the physical time of filling can be determined from the above-given formulas, the value of τ_0 being known. Note, theoretically, the time of filling of the second chamber equals infinity. In reality, however, this time is limited to a reasonable value: when the pressure reaches, e.g., the value $p_{ch2}(\tau) = (0.98\text{–}0.99)p_{ch}(\tau = \infty)$, i.e., when the pressure equals approximately 98–99% of the value that would be reached at $\tau = \infty$. This time is assumed to be the theoretical time of filling of the second chamber under the assumptions listed above.

Figure 4 shows the increase in pressure as a function of the normalized time $\bar{\tau}$, which was calculated by Eq. (6). The value $0.99p_{ch2}(\tau = \infty)$ corresponds to $\bar{\tau} = 4.61$.

For the test conditions of the present experiments, namely, $V_{ch2} = 12$ dm^3, $F_{th} = 0.0133$ m^2, $R = 287$ J/(kg·K), $B = 0.685$ (air with $k = 1.4$), $\mu_{th} \approx 1$, and $T_{ch1,(0)} = 1000$–1100 K (see Fig. 2), we have $\tau_0 \approx 2.4$ msec. Thus, the time of filling $\tau = \bar{\tau}\tau_0$ of the second chamber examined should be approximately 11 msec.

Figure 5 shows the pressure in the second chamber as a function of the test time for some experiments with different positions of the throttling grid between the chambers. The time before the moment corresponding to the vertical bar determines the process of filling of the second chamber after breakdown of diaphragm 4 (Fig. 1).

For all experiments, the time of filling of the second chamber, depending on the position of the throttling grid 5 between the chambers is given in Table 1. It is seen from Table 1 that the second chamber was filled by the time $\tau = 9$–14 msec in all experiments except for those where the throttling grid was in the position 5a. In the latter case, this time was considerably smaller and equal to 4–5 msec.

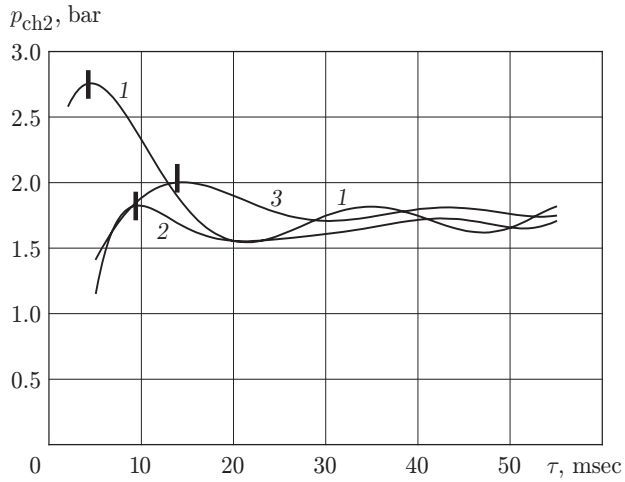

Fig. 5. Pressure in the second chamber versus the test time with different positions of the throttling grid between the chambers: curves 1–3 refer to the positions 5a, 5c, and 5d (Fig. 1), respectively; the vertical bars indicate the time when the second chamber is filled.

TABLE 1

Time of Filling of the Second Chamber

Position of the throttling grid (number in Fig. 1)	Number of tests	τ_{st}, msec	τ_{tot}, msec	$\bar{\tau} = \tau/\tau_0$
5a	2	4–5	4	1.9
5b	4	13–14	11–14	4.6–5.8
5c	3	9–10	9–11	3.8–4.6
5d	2	12–14	11–14	4.6–5.8

Note. τ_{st} and τ_{tot} are the times of filling of the second chamber, determined from the measurements of static and total pressure, respectively.

Thus, we can draw the following conclusions on the time of filling of the second chamber from the analysis of test results.

1. If the throttling grid F_{1-2} is located downstream of the diaphragm (positions 5c and 5d in Fig. 1) or upstream of the diaphragm (position 5b in Fig. 1) but there is practically no empty volume between the throttling grid and the diaphragm, the time of filling of the second chamber obtained in experiments (9–14 msec) is in good agreement with the time predicted by the quasi-steady theory of filling and emptying of the second chamber (approximately 11 msec).

2. If the throttling grid F_{1-2} is located upstream of the diaphragm and there is some volume between them (see position 5a in Fig. 1), the experimentally obtained time of filling of the second chamber (4–5 msec) is twice lower than the value predicted by the quasi-steady theory. The reason is as follows.

The volume between diaphragm 4 and the throttling grid in the position 5a was 0.24 dm^3. For the diaphragm to be broken, this volume (after the capacitor discharge) should be filled approximately to a pressure of 300 bars. After diaphragm breakdown, the mass of the test gas enclosed in this volume is exhausted into the second chamber almost without any resistance because the throttling grid is located upstream, i.e., this mass that passed the throttling grid before diaphragm breakdown flows very rapidly into the second chamber volume, thus, decreasing the time of its filling.

3. By changing the volume between the throttling grid 5a and diaphragm 4, it is possible to control the time of filling of the second chamber and reduce it, as compared to the value predicted by the quasi-steady theory.

Pressure Peak due to Filling of the Second Chamber. The second chamber is filled to a pressure slightly higher than the pressure established during the test time. This is clearly seen from experiments where the filling occurred more rapidly, owing to the volume between the throttling grid 5a and diaphragm 4. In other experiments, where the throttling grid was in the positions 5b, 5c, or 5d, this phenomenon was also observed, though to a smaller extent, which can be seen, e.g., by comparing curves 2 and 3 with curve 1 in Fig. 5.

Such an "overfilling" of the second chamber is mainly caused by two factors.

1. As the gas flows from a volume with a higher pressure to a volume with a lower pressure, the temperature in the latter increases, as compared to the gas temperature in the first volume. This occurs owing to adiabatic compression of the gas in the second volume [17–19]. Since the gas flow rate through an arbitrary cross section is inversely proportional to the square root of stagnation temperature $G \approx 1/\sqrt{T_0}$, gas exhaustion from the second volume is "decelerated."

2. After diaphragm breakdown, a powerful shock wave passes in the channel between the plenum chambers. A zone with pressure and temperature several times higher than those in the first chamber is formed near the frontal edge of the channel, behind the reflected shock wave. The elevated pressure and temperature favor more rapid filling of the second chamber. Though the zone with elevated parameters in the region of the front wall of the channel exists for a limited time, this factor (due to very high parameters of the gas in this zone) also affects the character of filling of the second chamber.

Oscillations of Pressure in the Second Chamber. As is seen from Figs. 3 and 5, the pressure in the second chamber has an oscillatory component with both low and high frequencies. Possible reasons for that are oscillations of the gas column in the channel between the chambers, oscillations of supersonic jets entering the second chamber, and acoustic noise of supersonic jets. In the first experiments, in which an additional throttling grid 6 with 143 orifices 5 mm in diameter was mounted in the second chamber, there was a supercritical pressure difference on this grid. Therefore, it could serve as a source of aerodynamic noise.

In experiments where the diameter of orifices in grid 6 was increased to 14.5 mm, the size of orifices was too large to damp oscillations. Such a size of orifices was chosen to provide the value $\zeta = 2$–2.5, which is reached at $f \approx 0.5$. The value $f \approx 0.5$ in the grid already made could be achieved only by increasing the orifice diameter from 5 to 14.5 mm. In addition, the grid was rather thick because it was initially intended for throttling (and hence, had to sustain large pressure differences) rather than for equalization. Damping inhomogeneities is more effectively provided by thin grids [12].

In all cases, to reduce the amplitude of oscillations, one can decrease the length of the channel between the chambers or decrease the cell size in the grid in the second chamber because the velocity nonuniformity damped by the grid is three cell sizes or more [12].

Thermal Resistance of the Throttling Grid. All experiments were performed with a throttling grid made of copper. To determine the thermal resistance of small orifices in the throttling grid, two experiments were performed with a grid made of structural steel. The experiments were performed with the pressure multiplier. The temperature and pressure in the first chamber (hence, upstream of the throttling grid) were $T_{\text{ch1}} \approx 1000$ K and $p_{\text{ch1}} \approx 300$ bars. In the first experiment with the steel throttling grid, no noticeable burnout of orifices during the test time was observed. Already in the second experiment, however, the orifices started to burn out, which is clearly reflected by the pressure curve (Fig. 6): an increase in pressure is observed at $\tau \approx 35$ msec. It is not possible to determine the beginning of orifice burnout by the value of p_{ch1} because the pressure multiplier sustains a constant pressure in the first chamber despite the increasing area of orifices F_{1-2}. This is true until a certain value of F_{1-2} is reached after which the pressure multiplier is no longer able to sustain a constant pressure p_{ch1} and it starts to decrease owing to further burnout of orifices in the throttling grid. As is seen from Fig. 6, this occurs at $\tau = 60$–70 msec.

Thus, at $T_{\text{ch1}} \approx 1000$–$1100$ K and $p_{\text{ch1}} \approx 300$ bars, the steel grid with orifices 3.8 mm in diameter can withstand one or two experiments. With the same parameters upstream of the copper throttling grid, the orifices of the same diameter were not damaged. The reason is that the thermal conductivity of copper is nine times higher than the thermal conductivity of steel whereas their heat capacities are roughly identical. The heat flux toward the walls of the orifices of the throttling grid made of copper propagates inward the metal and does not lead to overheating of surface layers. In the case of the steel grid, because of its lower thermal conductivity, the heat flux leads to loss of strength of surface layers, which are blown off by the high-pressure sonic flow.

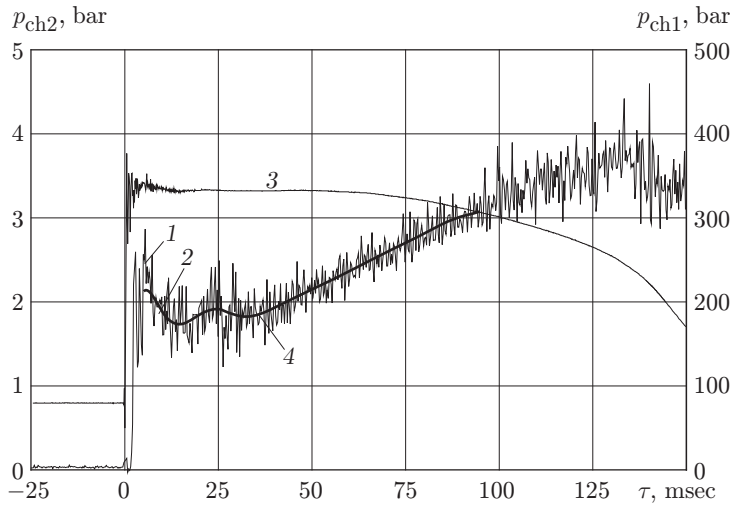

Fig. 6. Pressure in the chambers versus the test time: 1, 2) pressure in the second chamber (curves 1 and 2 show the measured values and approximation, respectively); 3) pressure in the first chamber (without approximation); 4) beginning of burnout of orifices of the throttling grid.

Parameters of the Test Gas in the Second Chamber. After the transitional processes are completed, a quasi-steady flow is formed in the gas-dynamic path of the wind tunnel. Despite some oscillatory phenomena, the parameters in the second chamber can be approximated by a smooth curve, which was chosen to be a polynomial of power $n = 5$–10 (see, e.g., Figs. 3, 5, and 6).

In the experiments performed, the ratio of static to total pressures in cross section No. 8 of the second chamber (Fig. 1) was 0.96–0.98. For $k = 1.33$, this corresponds to the Mach number in the second chamber $\mathrm{M} \approx 0.2$. The same value is obtained from the dependence $\mathrm{M} = f(d_{ch2}/d_{th})$. This is a comparatively large Mach number for the second chamber, which is a consequence of the small ratio $d_{ch2}/d_{th} = 1.77$ (lower than that normally recommended for wind tunnels [9]); here, $d_{ch2} = 230$ mm is the second-chamber diameter. Therefore, conducting experiments with $d_{ch2}/d_{th} \approx 1.8$ requires the use of a total pressure probe, and the test-gas parameters in the second chamber should be determined by the measured stagnation pressure.

The coincidence of the experimental value of the Mach number obtained from the ratio of static and total pressures and the Mach number calculated from the ratio d_{ch2}/d_{th} indirectly evidences that the flow in the cross section where the pressures are measured is already decelerated after the supersonic inflow into the chamber and is rather uniform over the cross section.

Figure 7 shows the ratio p_{ch1}/p_{ch2}. Under the assumption of an ideal gas and flow-rate coefficients equal to unity, the following relation should be valid in the quasi-steady regime after filling of the second chamber, as it follows from Eq. (4):

$$\frac{p_{ch1}(\tau)}{p_{ch2}(\tau)} = \frac{\mu_{th} F_{th}}{\mu_{1-2} F_{1-2}} = 167. \tag{7}$$

It is seen from Fig. 7, however, that the experimental value is $p_{ch1}/p_{ch2} = 200$–220. The main reason for the disagreement is the different flow-rate coefficients at the exit of the first and second chambers. For the second chamber, we can rather definitely assume that there are no pressure losses from the measurement point to the nozzle-throat cross section, and the flow-rate coefficient is $\mu_{th} = 1$. In the first chamber, there are losses in pressure between the pressure-measurement point and the throat cross section at the exit. In addition, the flow-rate coefficient in the throat cross section at the exit of the first chamber (i.e., throttling grid) is smaller than unity. The combination of these factors is responsible for the fact that the real pressure ratio is higher than the value obtained under the assumption of an ideal flow. Strictly speaking, in calculating the ratio p_{ch1}/p_{ch2}, one should take into account the test-gas compressibility. In the experiments conducted, however, the combination of pressures and temperatures was such (see Figs. 2 and 3) that this coefficient was almost constant over the second chamber duct and was close to unity. Therefore, this factor was ignored in Eq. (6).

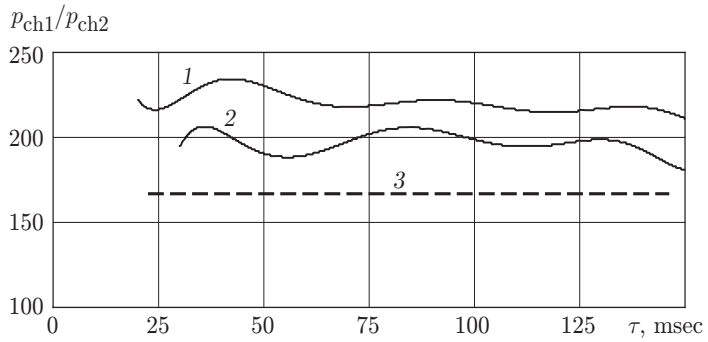

Fig. 7. Ratio of pressures in the first and second chambers: curves 1 and 2 show the approximations of experimental data for the throttling grid in the position 5d (1) and 5a (2); curve 3 is the calculation by Eq. (7).

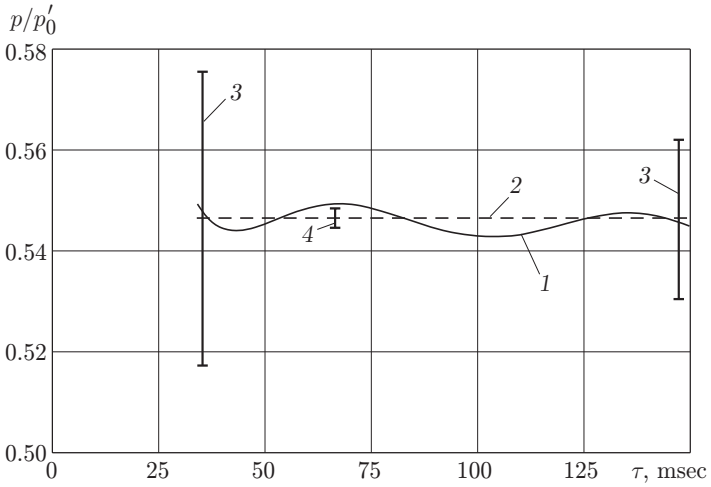

Fig. 8. Ratio p/p_0' versus the test time: 1) mean value for seven ratios of the approximated static pressure in the nozzle throat to the approximated total pressure at the nozzle exit; 2) mean value for the interval $\tau = 34$–160 msec for the data described by curve 1; 3) root-mean-square deviation for seven measured p/p_0'; 4) root-mean-square deviations for the data described by curve 1.

Flow at the Exit of the Second Chamber. Figure 8 shows the ratio of the static pressure in the nozzle-throat cross section to the stagnation pressure measured by the total pressure rake (see Fig. 1) at the exit of the second chamber. The pressure ratio remains almost constant during the entire test time (after the transitional process of filling of the second chamber), and the mean value is $p/p_0' = 0.546$ for $\tau = 34$–160 msec. At a temperature of 1000–1100 K, the ratio of specific heats for air is $k = 1.33$–1.34 [20]. With allowance for the scatter of experimental points, the experimentally obtained root-mean-square deviation of p/p_0' during the test time ($\sigma = 0.02$–0.028) corresponds almost exactly to the Mach number M = 1 (for M = 1 and $k = 1.33$, the calculated value of p/p_0' is 0.5404).

Based on the analysis of the data in Fig. 8, which were obtained in an experiment with the second-chamber configuration shown in the lower figure in Fig. 1, and data of similar experiments, we can conclude that the presence of a large-volume stagnant zone allows a rather uniform distribution of the flow entering discretely with a supersonic velocity. Hence, even for a pressure difference $p_{ch1}/p_{ch2} \approx 200$, there is no need to install an additional throttling grid in the second chamber. At the same time, the equalizing grid can make the flow more uniform. The cells of this grid should be as small as possible [12].

Some Comments on Experimental Data Processing. Approximation of the pressure $p_{\text{ch1}}(\tau)$ in the interval of τ from 5–10 to 140–160 msec is required only to determine the pressure $p_{\text{ch1},(0)}$ immediately after heat addition by extrapolating the experimental dependence to the time $\tau = 0$. This is necessary to calculate the temperature $T_{\text{ch1},(0)}$ and all parameters in the chamber during the test time [6]. There is no need for approximating the pressure in the first chamber for the analysis because the measurement system registers smooth values of p_{ch1} at $\tau > 5$–10 msec, when the oscillatory wave processes caused by the powerful electric discharge decay (see curves 1–3 in Fig. 2 and curve 3 in Fig. 6).

All static and total pressure probes in the second chamber and at its exit register oscillatory processes with low-frequency and high-frequency components (see Fig. 3). The root-mean-square deviation of the high-frequency component from the mean value is rather large: up to 15%. This generates problems in analyzing quantities depending on the pressure ratio (e.g., Mach numbers). By using values directly registered by the measurement system for such an analysis, one can obtain physically unrealistic values for some time instants. Therefore, the high-frequency component should be smoothed, e.g., by a power polynomial. This, however, involves difficulties in choosing the polynomial power n and the interval $[\tau_1, \tau_2]$ where the approximation is performed.

If the values $n = 1$–3 are chosen, the low-frequency component vanishes. At the same time, the analysis shows that low-frequency oscillatory phenomena can arise in the long channel between the chambers in the course of filling and emptying of the chambers.

For $n > 5$–6, the low-frequency component is retained. Nevertheless, there may be a certain phase shift for different measured values of pressures. For instance, the oscillatory character of curve 1 in Fig. 8, which shows the ratio of the static pressure in the throat cross section to the stagnation pressure, is caused by such a phase shift between the approximated static pressure and approximated stagnation pressure measured by total pressure probes in the rake. The oscillatory character of curve 1 in Fig. 8 contradicts the quasi-steady character of the nozzle flow because the nozzle flow is determined only by the nozzle contour and by the ratio of cross-sectional areas; in the zero-dimensional approach used in the present work, it should be independent of the pressure ratio. By comparing bars 3 and 4, one can verify that the root-mean-square deviation of the values on curve 1 from the mean value shown by curve 2 is an order of magnitude smaller than the root-mean-square deviation of the measured values of p/p'_0, i.e., an order of magnitude lower than the measurement accuracy. Therefore, we can ignore the form of curve 1 and assume that the experimental ratio of the static pressure in the throat cross section to the stagnation pressure corresponds to curve 2.

At the same time, the pressure ratio in Fig. 7 correctly describes the character of the oscillatory process in the channel between the chambers because the quantity p_{ch1} in the numerator has no oscillatory component (see Fig. 2).

The interval $[\tau_1, \tau_2]$ on which approximation is performed also affects the form of the approximation curve (see, e.g., Fig. 3). In the present work, the choice of the interval $[\tau_1, \tau_2]$ corresponded to the problem posed in analyzing experimental data. In examining the process of filling of the second chamber, the initial interval up to $\tau = 30$–60 msec was chosen. In studying the flow in the quasi-steady regime, the initial interval was eliminated. Such a choice of the interval $[\tau_1, \tau_2]$ offered the best possibilities of tracking the pressure variation in the conducted experiments.

Conclusions. 1. The time of filling of the second chamber is in overall agreement with the data calculated in the quasi-steady approximation and reaches 9–14 msec for the chamber tested. The quantity $\bar{\tau}$ can serve as a similarity criterion. The physical time of filling of the second chamber is determined from $\bar{\tau}$ and from the value of τ_0 depending on the chamber geometry and test-gas parameters in the first chamber.

2. Wave processes in the transitional channel have a strong effect on the character of filling of the second chamber.

3. If the channel elements between the chambers are located in the sequence "grid of the impingement plate of the high-pressure chamber → diaphragm → throttling grid F_{1-2}", it is desirable to have a minimum structurally possible distance between the diaphragm and the throttling grid to avoid adverse influence of wave processes.

4. If the throttling grid is located upstream of the diaphragm, the time of filling of the second chamber can be reduced by increasing the volume between the throttling grid and the diaphragm. In the conducted experiments, this volume (0.24 dm^3) allowed a twofold decrease in the time of filling of the second chamber of volume $V_{\text{ch2}} = 12$ dm^3: from 9–14 msec to 4–5 msec.

5. The pressure peak observed in the course of filling of the second chamber ("overfilling") is associated with test-gas overheating during the filling of the second chamber and with wave processes in the transitional channel.

6. For air temperatures in the first chamber $T_{ch1} \approx 1000$ K and pressures $p_{ch1} \approx 300$ bars, the orifices 3.8 mm in diameter in the throttling grid made of steel burn out during one or two experiments. With the same parameters upstream of the copper throttling grid, the orifices of the same diameter are not damaged.

7. Even for a pressure difference between the chambers $p_{ch1}/p_{ch2} \approx 200$, there is no need in an additional throttling grid in the second chamber. In a large volume of the stagnant zone in the second chamber, the flow entering discretely with a supersonic velocity is distributed rather uniformly. The equalizing grid should have cells of the smallest possible size to effectively damp flow nonuniformities.

REFERENCES

1. R. I. Kurziner, *Reactive Engines for High Supersonic Flight Velocities* [in Russian], Mashinostroenie, Moscow (1989).
2. E. S. Shchetinkov, *Physics of Combustion and Explosion* [in Russian], Nauka, Moscow (1965).
3. V. K. Baev, V. V. Shumskii, and M. I. Yaroslavtsev, "Force characteristics and flow parameters in combustion models," *J. Appl. Mech. Tech. Phys.*, **25**, No. 1, 93–97 (1984).
4. V. K. Baev, V. V. Shumskii, and M. I. Yaroslavtsev, "Study of combustion and heat exchange processes in high-enthalpy short-duration facilities," in: S. N. B. Murthy and E. T. Curran, *Progress in Astronautics and Aeronautics*, Vol. 137: *High-Speed Flight Propulsion Systems* (1991), pp. 457–480.
5. V. V. Kislykh and Kh. A. Rakhmatullin, "Double-chamber adiabatic-compression facility," *Teplofiz. Vysok. Temp.*, **10**, No. 2, 400–404 (1972).
6. A. S. Korolev, B. V. Boshenyatov, I. G. Druker, and V. V. Zatoloka, *Hotshot Wind Tunnels in Aerodynamic Research* [in Russian], Nauka, Novosibirsk (1978).
7. L. N. Puzyrev and M. I. Yaroslavtsev, "Stabilization of gas parameters in the plenum chamber of a hypersonic hot-shot wind tunnel," *Izv. Sib. Otd. Akad. Nauk SSSR, Ser. Tekh. Nauk*, No. 5, 135–140 (1990).
8. V. V. Shumskii, "Chemical heating and adiabatic compression used in high-enthalpy facilities to extend the range of studying gas-dynamic models with combustion," *ibid.*, pp. 149–157.
9. I. A. Panichkin and A. B. Lyakhov, *Fundamentals of Gas Dynamics and Their Application to Wind-Tunnel Calculations* [in Russian], Izd. Kiev. Univ., Kiev (1965).
10. M. E. Topchiyan and A. M. Kharitonov, "Wind tunnels for hypersonic research (progress, problems, and prospects)," *J. Appl. Mech. Tech. Phys.*, **35**, No. 3, 383–395 (1994).
11. Yu. P. Goonko, V. I. Zvegintsev, I. I. Mazhul, et al., "Wind-tunnel testing of a hypersonic scramjet model at high Mach and Reynolds numbers," *Teplofiz. Aéromekh.*, **10**, No. 3, 321–345 (2003).
12. G. I. Taganov, "Equalizing effect of the grid in liquid and gas flows," *Tr. TsAGI*, No. 604 (1947).
13. I. E. Idel'chik, *Handbook on Hydraulic Resistances* [in Russian], Mashinostroenie, Moscow (1975).
14. I. E. Idel'chik, "Investigation of wind-tunnel nozzles," *Tekh. Zamet. TsAGI*, No. 80 (1935).
15. M. E. Deich and A. E. Zaryankin, *Hydrogasdynamics* [in Russian], Énergoatomizdat, Moscow (1984).
16. V. I. Pinakov, V. N. Rychkov, and M. E. Topchiyan, "Possibility of simulating hypersonic flows on high-pressure adiabatic gas-dynamic compression setups," *J. Appl. Mech. Tech. Phys.*, **23**, No. 1, 56–61 (1982).
17. O. V. Lyzhin and A. L. Iskra, "Process of emergency depressurization of a vacuum chamber," *Tr. TsAGI*, No. 1046 (1969).
18. E. I. Sosnin, "Variation of gas parameters in the course of filling and emptying of reservoirs," *Tr. TsAGI*, No. 1786 (1976).
19. V. M. Antokhin and V. A. Zhokhov, "Gas-overheating phenomenon in a hotshot wind tunnel," *Uch. Zap. TsAGI*, **16**, No. 2, 41–49 (1985).
20. N. B. Vargaftik, *Handbook on Thermophysical Properties of Gases and Liquids* [in Russian], Nauka, Moscow (1972).